Assessment of Higher–Order Forces on a Vertical Cylinder with Decomposition Model Based on SWENSE Method

Vuko Vukčević[1], Hrvoje Jasak[1] and Šime Malenica[2]

[1] *University of Zagreb, Zagreb/Croatia, {vuko.vukcevic, hrvoje.jasak@fsb.hr}*
[2] *Bureau Veritas, Paris/France, sime.malenica@bureauveritas.com*

1 Summary

Off–shore structure design often relies on accurate assessment of higher–order forces because of ringing phenomena. In this work, calculation of higher–order forces on a vertical surface piercing cylinder is carried out by a decomposition CFD model based on Spectral Wave Explicit Navier–Stokes (SWENSE) approach [1]. First, mesh and time refinement studies are carried out for a case with intermediately steep ($ka = 0.12$) incoming wave train. Second, a set of waves with different frequencies are simulated, keeping the wave steepness constant, $ka = 0.06$. Higher–order forces up to fourth order are compared with fully non–linear potential flow results [2]. A discussion on strong second order behaviour of vorticity effects in the vicinity of the cylinder is presented.

2 Introduction

CFD models based on Reynolds–Averaged Navier–Stokes (RANS) equations are progressively gaining attention in the marine industry [4] due to increase in computational resources and their ability to tackle non–linear, coupled equation sets. However, verification and validation of RANS models is still under–way [3], both for steady and transient phenomena. Transient simulations demand more CPU time compared to steady state simulations, making them more expensive to verify in terms of grid refinement and other sensitivity studies.

In this paper, we shall simulate wave diffraction problem in regular waves and assess the higher–order forces exerted on a vertical surface–piercing cylinder with a recently developed decomposition model based on SWENSE [1] method. The model is implemented in foam–extend, a fork of OpenFOAM computational continuum mechanics software. Validation of the model shall be achieved by comparing the results with fully non–linear potential flow, time–domain simulation by Ferrant et al. [2]. In order to verify the presented method, time–step and mesh refinement studies will be carried out for a representative test case.

3 Approach

The mathematical model of the incompressible, viscous, two–phase flow is modelled with momentum (Navier–Stokes) and phase continuity equations. Interface capturing is achieved with implicitly redistanced Level Set method [5] reformulated in a form suitable for Finite Volume (FV) discretisation [6]. The method does not need additional explicit redistancing. In order to efficiently model incoming waves, solution is decomposed into incident and diffracted fields following Ferrant et al. [1]. The method presented here is more general in a sense that diffracted field may contain additional phenomena not taken into account by incident wave field, such as:

viscosity, vorticity, two–phase effects, radiation effects, etc. Hence, perturbation around incident wave field is calculated via fully non–linear, viscous, two–phase equation set in the present CFD model. As a consequence, incident wave field is explicit in the CFD calculation, facilitating wave transport [7]. Governing equations are briefly presented, the reader is referred to Vukčević and Jasak [6] for detailed derivation:

- Volumetric continuity equation:

$$\nabla \bullet \mathbf{u}_D = -\nabla \bullet \mathbf{u}_I \,, \tag{1}$$

  where $\mathbf{u}_D$ is the diffracted velocity field, and $\mathbf{u}_I$ is the incident wave field. We stress that index D denotes perturbation around incident (I) field, modelling vorticity, viscosity, diffraction and possibly radiation effects.

- Momentum equation:

$$\begin{aligned} \frac{\partial(\rho \mathbf{u}_D)}{\partial t} + \nabla \bullet (\rho \mathbf{u}\mathbf{u}_D) - \nabla \bullet (\mu_{eff} \nabla \mathbf{u}_D) = -\frac{\partial(\rho \mathbf{u}_I)}{\partial t} - \nabla \bullet (\rho \mathbf{u}\mathbf{u}_I) + \nabla \bullet (\mu_{eff} \nabla \mathbf{u}_I) \\ - \nabla p_d - \mathbf{g} \bullet \mathbf{x} \nabla \rho + \nabla \mathbf{u} \bullet \nabla \mu_{eff} + \sigma \kappa \nabla \alpha \,, \end{aligned} \tag{2}$$

  where ρ is the mixture density, μ_{eff} effective viscosity of the mixture, p_d dynamic pressure, $\mathbf{g}$ gravitational acceleration, $\mathbf{x}$ position vector, σ surface tension coefficient, κ curvature of the free surface and α is the volume fraction.

- Level Set equation derived from Phase Field method [5]:

$$\begin{aligned} &\frac{\partial \psi_D}{\partial t} + \nabla \bullet (\mathbf{c}\psi_D) - \psi_D \nabla \bullet \mathbf{c} - b \nabla \bullet (\nabla \psi_D) = \\ &- \frac{\partial \psi_I}{\partial t} - \nabla \bullet (\mathbf{c}\psi_I) + \psi_I \nabla \bullet \mathbf{c} + b \nabla \bullet (\nabla \psi_I) + b \frac{\sqrt{2}}{\epsilon} \tanh\left(\frac{\psi}{\epsilon\sqrt{2}}\right) \,, \end{aligned} \tag{3}$$

  where ψ denotes Level Set field, $\mathbf{c}$ convective flux [6], b stabilisation parameter and ϵ denotes smearing distance.

Wave reflection is prevented using implicit relaxation zones [6], where the diffracted field is forced to vanish near the boundaries, leaving full potential flow solution.

Numerical discretisation of governing partial differential equations, (1), (2) and (3) is achieved with second–order accurate, polyhedral FV method in foam–extend. Terms related to incident wave field are discretised explicitly as they are known at each time–step, while diffracted fields are solved in implicit manner. Temporal discretisation is achieved via blend of Euler and Crank–Nicholson schemes. Convective terms are discretised either with second–order accurate linear upwind scheme (for momentum) or with Van Leer's TVD scheme (other convective terms). Diffusion terms are discretised using central differencing. Pressure–velocity–free surface coupling is achieved with a PIMPLE aglorithm, a combination of SIMPLE and PISO algorithms.

4 Cylinder diffraction

Diffraction of a 3–D vertical, surface piercing cylinder due to regular wave train is simulated. A deep water wave with intermediate steepness $ka = 0.12$ (Table 1 presents other geometrical and wave properties) is chosen as a benchmark test case. Block–structured mesh extends two wave lenghts in the radial direction, while the symmetry plane is used to lower the CPU time. The cells are heavily graded towards the free surface and the cylinder. There are 120 cells per wave length in the area near the cylinder and 20 cells per wave height, while the maximum aspect ratio is 166.7. The mesh consists of 552 000 cells.

Table 1: Geometry and wave parameters for the benchmark case.

Cylinder radius	r, m	1
Wave number–depth parameter	kd	8
Wave number–radius parameter	kr	0.2
Wave amplitude–depth parameter	a/d	0.015
Wave steepness parameter	ka	0.12

4.1 Time resolution study

Time resolution study has been carried out by chaning the Courant–Friedrichs–Lewy (CFL) number from 5 ($\approx$ 140 time–steps per period) to 0.125 ($\approx$ 1600 time–steps per period). 10 periods were simulated and the frequency domain analysis has been made via moving window FFT. The statistically averaged inline force harmonics are calculated as the average of the last 9 periods. The first period was excluded due to simulation start up. In–line forces are presented in dimensionless form following Ferrant et al. [2]. ρ is set to 1000 kg/m^3 and g is 9.81 m/s^2. Results of the time resolution study are presented in Figure 1. Figure 1a presents the normalized force harmonic coefficients for different CFL numbers, while Figure 1b presents relative errors compared to Ferrant et al. [2]. Relative errors for smallest CFL number are presented in Table 2. First, third and fourth order forces have a relative error less than 3%. Steady second order drift force has the largest error, 16%. Second order force has the error of approximately 12%.

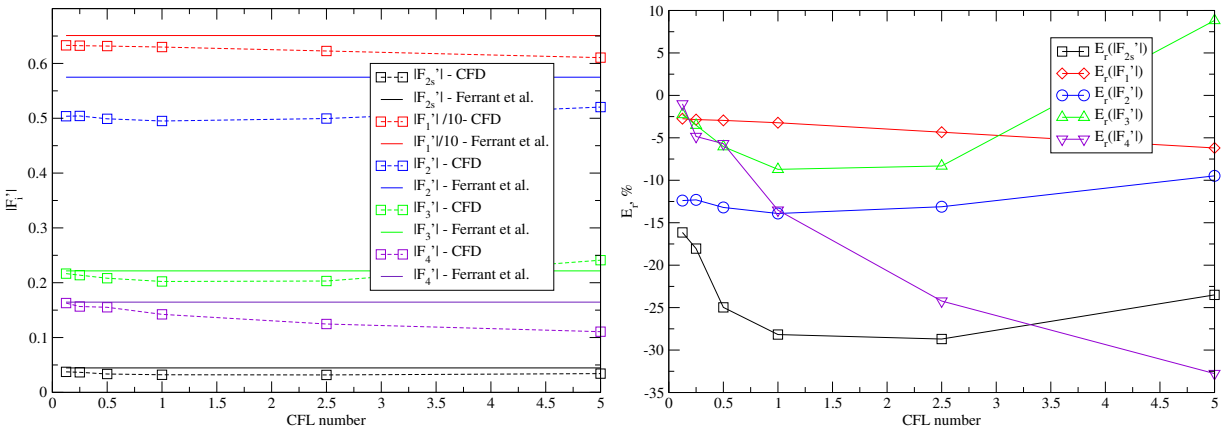

(a) Normalized force harmonics.

(b) Relative errors.

Figure 1: Vertical cylinder diffraction: time refinement study.

Table 2: Relative errors compared to Ferrant et al. (1999) [2] for $CFL = 0.125$ case.

$E_r(\lvert F_1'\rvert), \%$	$E_r(\lvert F_{2s}'\rvert), \%$	$E_r(\lvert F_2'\rvert), \%$	$E_r(\lvert F_3'\rvert), \%$	$E_r(\lvert F_4'\rvert), \%$
-2.75	-16.14	-12.39	-2.25	-1.00

4.2 Mesh refinement study

Mesh refinement study has been carried out using four meshes. Finer meshes have 25%, 50% and 75% more cells in each direction compared to the benchmark case. Same settings are used as in the previous subsection, while the CFL number was fixed at 0.25. Table 3 presents mesh refinement details. Figure 2a presents convergence of normalized force harmonics with respect to mesh refinement, while Figure 2b presents relative errors of higher order forces. It can be seen that the relative errors for higher order forces, namely third and fourth order forces exhibit oscillatory behaviour. Table 4 presents relative errors for the finest mesh.

Table 3: Mesh refinement study parameters.

Mesh refinement index	0	1	2	3
Cell count increase, %	0	25	50	75
Total cell count	552 000	1 005 700	1 854 000	2 964 500

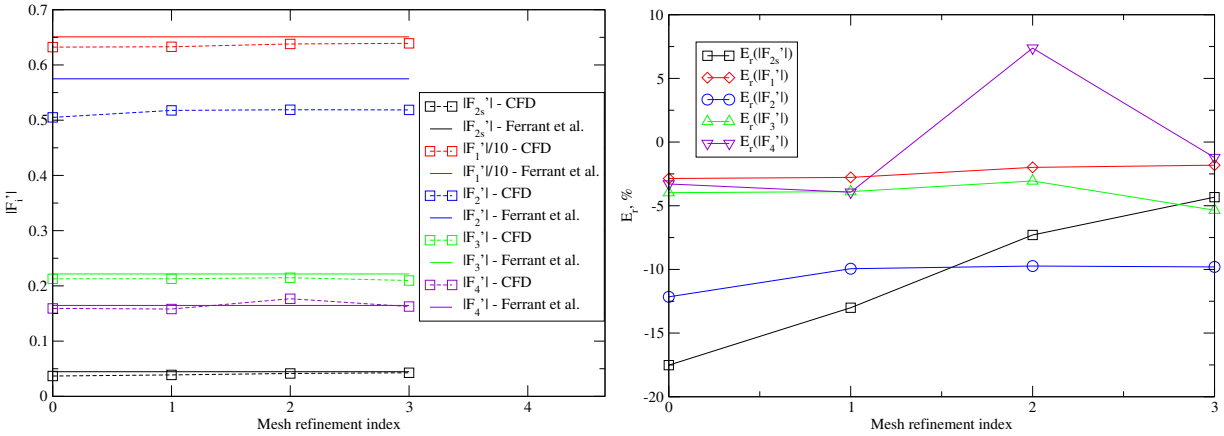

(a) Normalized force harmonics.

(b) Relative errors.

Figure 2: Vertical cylinder diffraction: mesh refinement study.

Table 4: Relative errors compared to Ferrant et al. (1999) [2] for the finest mesh.

$E_r(\lvert F_1' \rvert), \%$	$E_r(\lvert F_{2s}' \rvert), \%$	$E_r(\lvert F_2' \rvert), \%$	$E_r(\lvert F_3' \rvert), \%$	$E_r(\lvert F_4' \rvert), \%$
-1.82	-4.33	-9.80	-5.35	-1.22

4.3 Wave number study

Simulations were performed for a wave with a steepness of $ka = 0.06$, while Table 5 presents other geometrical and wave parameters. A different mesh is used for each case, such that the number of cells per wave height and length remains the same as in the base case. Figure 3 presents normalized forces for different wave number–radius parameter kr. Black, red and blue lines represent real, imaginary and absolute value of the harmonic, respectively. Observing real and imaginary parts, slight phase shift difference is revealed. The phase shift is larger for higher wave numbers, while the absolute values of the harmonics are in good agreement for all orders.

Table 5: Geometry and wave parameters for the wave number study.

Cylinder radius	r, m	1
Wave number–depth parameter	kd	8
Wave amplitude–depth parameter	a/d	0.0075
Wave steepness parameter	ka	0.06
Wave number–radius parameter	kr	0.05, 0.01, 0.15, 0.20, 0.25 and 0.30

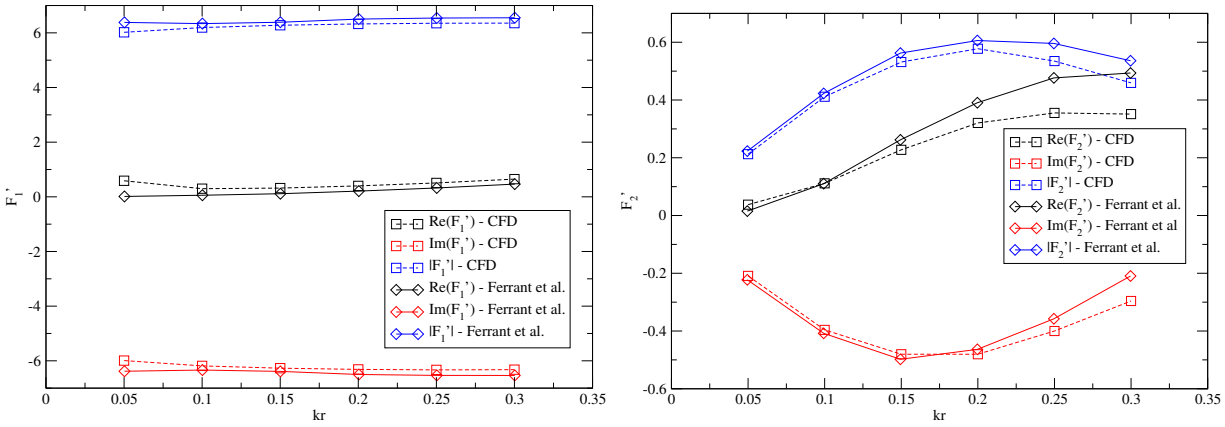

(a) Normalized first order harmonics.

(b) Normalized second order harmonics.

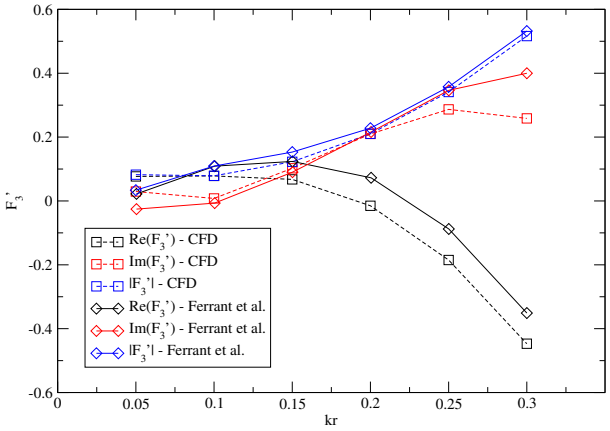

(c) Normalized third order harmonics.

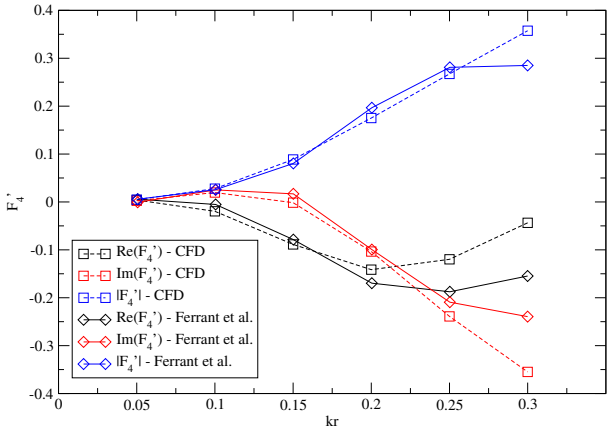

(d) Normalized fourth order harmonics.

Figure 3: Vertical cylinder diffraction: wave number study.

4.4 Vorticity effects

Vorticity effects are assessed by measuring enstrophy at three probes positioned closely in the front, at the side and in the back of the cylinder. Figure 4a presents enstrophy variation in time for three probes. The highest amount of vorticity is present at the side of the cylinder, which might be related to orthogonality of incident and diffracted waves in that region. Figure 4b presents same signals in frequency domain. Apart from the mean value, enstrophy at each probe exhibits significant second order behaviour. It was also observed that the magnitude of the enstrophy increases for higher frequencies: $kr = 0.05$ case measured enstrophy one order of magnitude smaller than the $kr = 0.3$ case. As the potential flow model does not take into account vorticity effects, authors believe that these effects are the reason for larger discrepancy for second order forces, especially for cases with higher frequency.

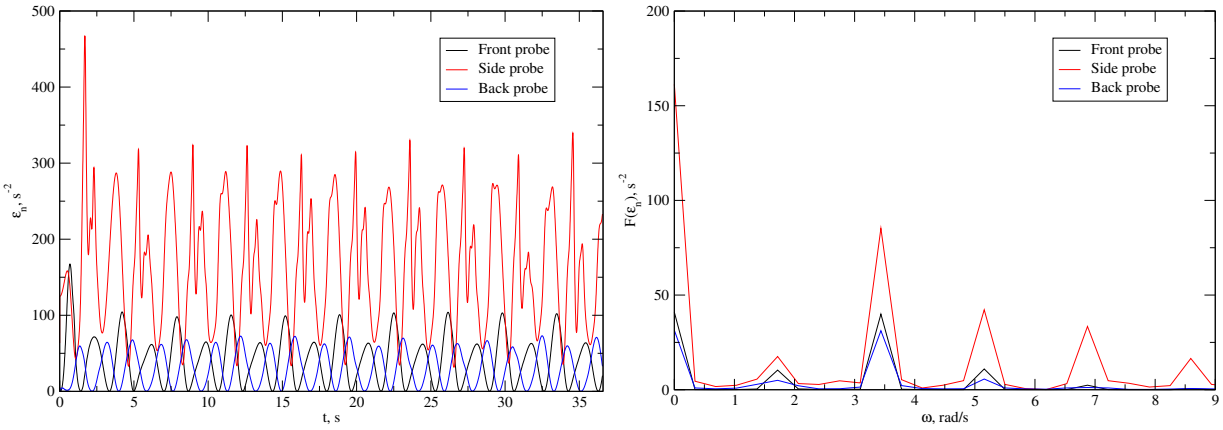

(a) Time domain.

(b) Frequency domain.

Figure 4: Enstrophy in the vicinity of the cylinder, $kr = 0.3$, $\omega = 1.718$ rad/s case.

4.5 Conclusion

Decomposition model based on SWENSE method, implicitly redistanced Level Set and implicit relaxation zones is briefly presented in this paper. Validation and verification of the model is carried out by assessing higher order forces on a circular, surface piercing cylinder. Time resolution and mesh refinement studies have been carried out for an intermediately steep wave $ka = 0.12$, showing good convergence. A set of simulations with different wave frequencies has been carried out. All results show satisfactory agreement compared to fully non–linear potential flow solution. A qualitative study of vorticity effects near the cylinder is also presented, revealing strong second order behaviour. Authors believe that vorticity effects could explain larger relative errors for second order forces, as the enstrophy is related to dissipation of the kinetic energy.

References

[1] P. Ferrant, L. Gentaz, and D. Le Touzé. A new RANSE/Potential Approach for Water Wave Diffraction. In *Proc. Numerical Towing Tank Symposium, NuTTS*, September 2002.

[2] P. Ferrant, Š. Malenica, and B. Molin. Nonlinear wave loads and runup on a vertical cylinder. In *Advances in Fluid Mechanics, Nonlinear Water Wave Interaction*. WIT Press, 1999.

[3] L. Larsson, F. Stern, and M. Vissoneau. *Numerical Ship Hydrodynamics: An assessment of the Gothenburg 2010 workshop*. Springer, 2013.

[4] F. Stern, J. Yang, Z. Wang, H. Sadat-Hosseini, M. Mousaviraad, Bhushan S., and T. Xing. Computational Ship Hydrodynamics: Nowadays and Way Forward. In *Proceedings of the 29th Symposium on Naval Hydrodynamics*, pages 1–73, August 2012.

[5] Y. Sun and C. Beckermann. Sharp interface tracking using the phase–field equation. *J. Comput. Phys.*, 220:626–653, 2007.

[6] V Vukčević and H. Jasak. Decomposition Model for Naval Hydrodynamic Applications, Part I: Computational Method. *Submitted to Ocean Engineering*, ??:???–???, 2015.

[7] V. Vukčević, H. Jasak, and Š. Malenica. Solution and Domain Decomposition Model for Naval Hydrodynamics: RANS and Potential Flow Coupling. In *VI International Conference on Computational Methods in Marine Engineering (MARINE 2015)*, pages 903–918, June 2015.